Exciton front propagation in photoexcited GaAs quantum wells

Sen Yang,[1] L. V. Butov,[1] L. S. Levitov,[2] B. D. Simons,[3] and A. C. Gossard[4]
[1]*Department of Physics, University of California at San Diego, La Jolla, California 92093-0319, USA*
[2]*Department of Physics, Massachusetts Institute of Technology, Cambridge, Massachusetts 02139, USA*
[3]*Cavendish Laboratory, Madingley Road, Cambridge CB3 OHE, United Kingdom*
[4]*Materials Department, University of California at Santa Barbara, Santa Barbara, California 93106-5050, USA*
(Received 20 August 2009; revised manuscript received 10 February 2010; published 16 March 2010)

We report on the study of spatiotemporal self-organization of carriers in photoexcited GaAs quantum wells. Propagating interfaces between electron-rich and hole-rich regions are seen as expanding and collapsing exciton rings in exciton emission patterns. The interfaces preserve their integrity during expansion, remaining as sharp as in the steady state, which indicates that the dynamics is controlled by carrier transport. The front propagation velocity is measured and compared to theoretical model. The measurements of expanding and collapsing exciton rings afford a contactless method for probing the electron and hole transport.

DOI: 10.1103/PhysRevB.81.115320 PACS number(s): 78.67.De, 71.35.−y, 72.20.−i, 78.55.Cr

I. INTRODUCTION

Front propagation in conducting media driven by injection or photoexcitation of carriers with opposite polarities is fundamental and ubiquitous in nature and technology. Diverse examples of moving interfaces resulting from self-organization of charge carriers range from traveling fronts of impact ionization in semiconducting structures[1–4] to transient dynamics in fuel cells.[5,6] The ability to control front propagation and spatial width is important in applications, including subnanosecond high-voltage pulse power ramps[1–4] and ignition of fuel cells.[5,6]

In this paper, we report on the study of expanding and collapsing exciton rings, formed at the boundaries between electron-rich and hole-rich regions in GaAs quantum wells. Such self-organization of excitons in steady-state ringlike patterns has been observed a few years ago[7] and thoroughly studied recently.[8–11] Here, we use spatiotemporal imaging of ring dynamics to measure its formation and propagation.

The real time imaging of expanding and collapsing exciton rings opens up several avenues of investigation. In this work, we demonstrate that the dynamics of exciton rings can be used for probing the electron and hole transport. Similar to other optical methods, this technique is contactless and therefore can be applied even when good contacts are difficult to make (see Ref. 12 and references therein). In particular, in this paper we study coupled electron-hole ($e-h$) layers separated by 4 nm barrier (12 nm between the centers of e and h layers). The task of making separate contacts to coupled $e-e$ or $e-h$ layers for transport measurements becomes challenging for systems with sub-10 nm barrier width. Yet, this is the most interesting regime, in which strong interlayer correlations can give rise to a variety of electronic states.[13–21]

As we shall see, the use of ring dynamics as a vehicle for studying carrier transport is made possible because ring expansion and collapse occur on time scales which are much longer than the ring formation time. The observation that exciton rings preserve their integrity during expansion and collapse shows that the characteristic times for the latter are much slower than those for self-organization of electrons, holes, and excitons into ringlike patterns.

In Sec. II, we present the experimental data on exciton front propagation in photoexcited GaAs quantum wells seen as expanding and collapsing rings in exciton emission patterns. In Sec. III, we summarize the transport model of exciton rings, developed in Ref. 8, which interprets the rings in terms of the boundaries between electron-rich and hole-rich regions. In Sec. IV, we compare experimental data with numerical simulations of the ring dynamics and use the measurements of the front propagation velocity for estimating the electron and hole diffusion coefficients. A short summary of the work is given in Sec. V. The unit calibration and fitting procedure are described in the Appendix.

II. EXPERIMENTAL RESULTS

The coupled quantum well structure (CQW) used in these experiments was grown by molecular beam epitaxy. It is comprised of two 8 nm GaAs QWs separated by a 4 nm $Al_{0.33}Ga_{0.67}As$ barrier and surrounded by 200 nm $Al_{0.33}Ga_{0.67}As$ layers (for details on the CQW see Ref. 7). The recombination lifetime of the indirect excitons in the CQW is about 50 ns.[23] The measurements were performed using time-resolved imaging with 200 ns integration window and 2 μm spatial resolution at $T=1.4$ K. The electrons and holes were photogenerated using rectangular excitation pulses of a semiconductor laser at 1.95 eV, above the $Al_{0.33}Ga_{0.67}As$ gap ($\sim$1.93 eV), with a 8 μm spot. The pulse width was 10 μs, with the edge sharpness better than 1 ns, and the repetition frequency of 67 kHz [Fig. 1(i)]. The period and duty cycle were chosen to provide time for the pattern to approach equilibrium during the laser pulse and to allow complete decay of the emission between the pulses. Different pulse widths and repetition frequencies were found to yield similar results. Time-dependent emission images were acquired by a nitrogen-cooled CCD camera after passing through a time-gated PicoStar HR TauTec intensifier with a time-integration window of 200 ns. An 800 ± 5 nm interference filter, chosen to match the indirect exciton energy, was used to remove the low-energy bulk emission and high-energy direct exciton emission. The spectral filtering and time-gated imaging provided the direct visualization of the

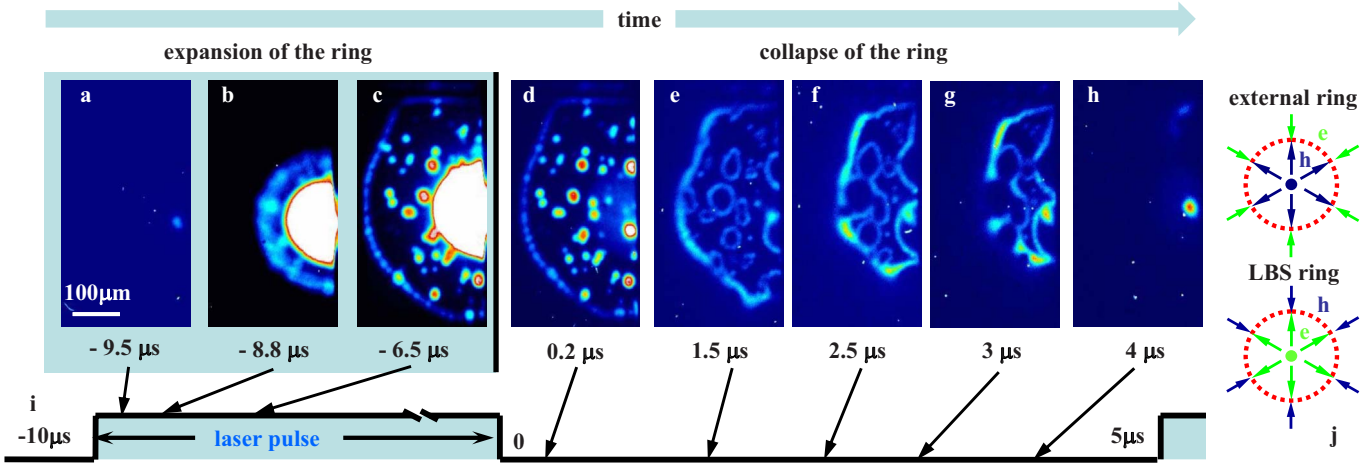

FIG. 1. (Color online) (a–h) Spatiotemporal exciton pattern formation. Emission images for indirect excitons at different time delays obtained with time-integration window of 200 ns. Zero time is chosen at the end of the laser pulse. Gate voltage V_g=1.235 V, laser peak power P_{ex}=1.82 mW. (i) Schematic of the laser pulse duty cycle sequence. (j) Schematic of carrier transport in the external ring and LBS ring (see text).

spatial intensity profile of the indirect exciton emission as a function of the delay time t after the laser pulse.

Figures 1(a)–1(h) show typical time evolution of the exciton emission pattern. After the start of a rectangular excitation pulse, the exciton ring expands [Figs. 1(a)–1(c)] approaching a steady state; simultaneously, several rings appear inside the expanding ring. These smaller rings are centered around the localized bright spots (LBS). They can be also seen in cw experiments (cf. Ref. 8). After the excitation pulse ends, the external ring collapses while the LBS rings expand [Figs. 1(d)–1(h)]. A movie showing the front propagation of the expanding and collapsing rings in the emission pattern of indirect excitons is presented in Ref. 24. The time evolution of the external ring radius for different values of excitation power P_{ex} and gate voltage V_g is shown in Figs. 2(a) and 2(b). To compensate for the deviation from perfect circular shape, the ring radius was estimated from the net area enclosed by the ring. The time evolution of the LBS-ring radius for different LBS and V_g is shown in Figs. 3(c) and 3(d).

III. MODEL

The observed dynamics was simulated using the model based on the in-plane spatial separation of electrons and holes.[8–11] The mechanism for the external ring formation can be summarized as follows. The electrons and holes, photo-

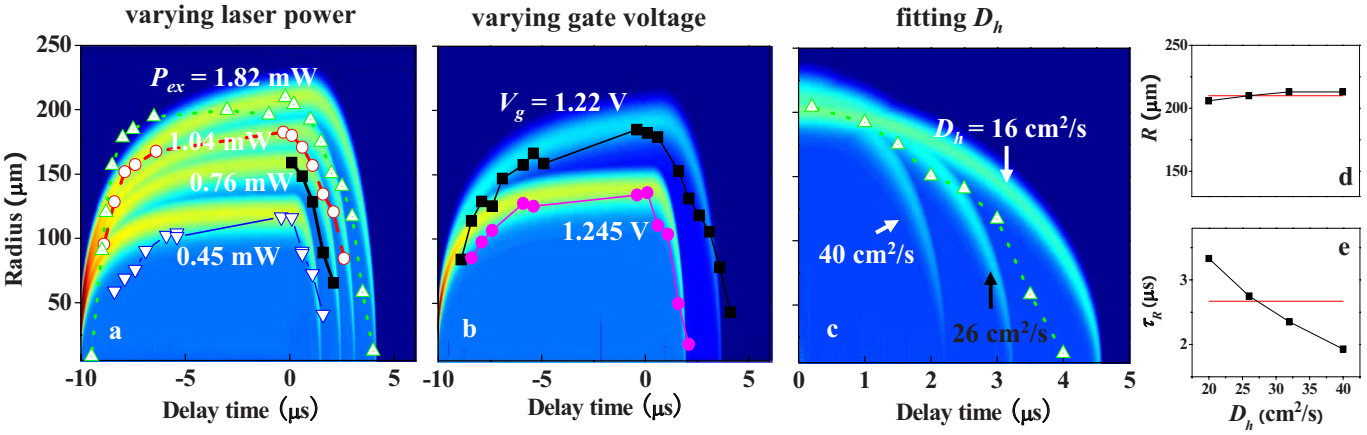

FIG. 2. (Color online) Expansion and collapse of the external ring. (a) Measured time dependence of the ring radius for several values of excitation power P_{ex}=0.45, 0.76, 1.04, and 1.82 mW at V_g=1.235 V (triangles, squares, circles), shown together with simulated dynamics, Eq. (1). Results of four different simulations are combined together, for hole source values I_p=17.5, 26.25, 32.5, and 42.5 (from bottom to top) and $\gamma=4.2\times10^6$ s^{-1} (for definition of units see Appendix). (b) Measured dynamics of the external ring radius for V_g=1.22 and 1.245 V at P_{ex}=0.76 mW (squares and circles) and simulated dynamics for different electron sources γ=2.85 (larger radius) and 5.4×10^6 s^{-1} (smaller radius) at I_p=26.25. The values of other parameters used in the simulations in (a,b) were kept fixed: D_e=80 cm^2/s, D_h=26 cm^2/s, n_b=1, and w=4. (c) Simulated dynamics for D_h=16, 26, and 40 cm^2/s and the measured dynamics for P_{ex} =1.82 mW with the rest of the parameters the same as in (a). The simulations are shifted so that t=0 corresponds to the time when the ring radius is maximum. The value D_h=26 cm^2/s gives the best fit to the measured dynamics. (d,e) Ring radius R and collapse time τ_R in simulations vs. D_h with the rest of the parameters the same as in (c) (squares). Red line marks the experimental result in (c).

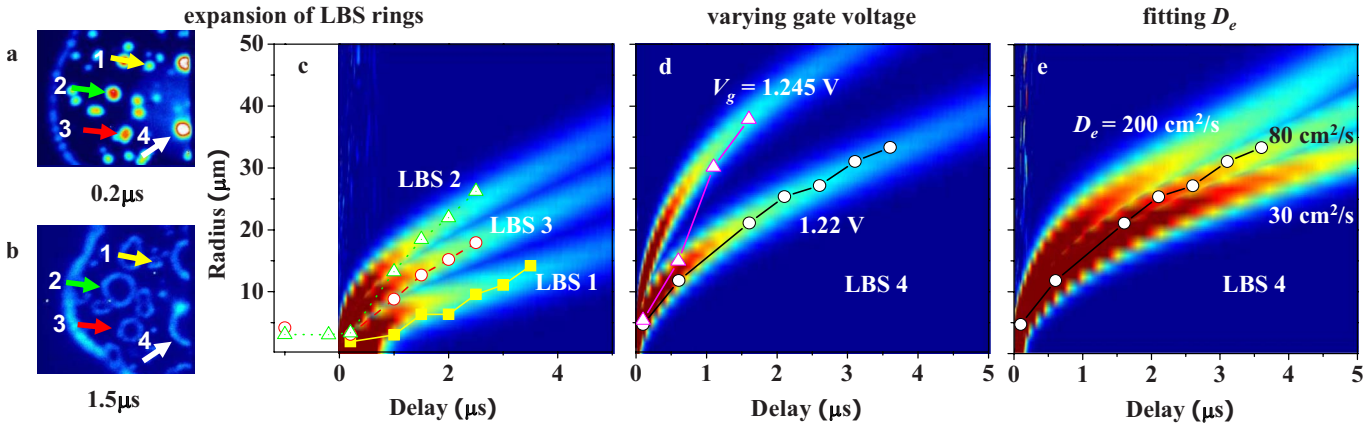

FIG. 3. (Color online) Dynamics of LBS rings. (a,b) Emission images for indirect excitons at time delays 0.2 and 1.5 μs after the laser pulse end. The arrows mark four LBS rings. (c) Measured dynamics of the ring radius for LBS 1, LBS 2, and LBS 3 [yellow, green, and red arrows in (a,b)] at V_g=1.235 V and P_{ex}=1.82 mW (squares, triangles, circles). Note that the brighter LBS in (a) expands faster. Simulated dynamics for different electron source values at the LBS center n_{bc}=4000, 7000, and 8400 (from bottom to top), n_{bo}=0.05 away from the LBS center, and the hole density at the pulse end p_b=10 (color scale curves). (d) Measured dynamics of ring expansion for LBS 4 [white arrow in (a,b)] for V_g=1.22 and 1.245 V at P_{ex}=0.76 mW (circles, triangles) and simulated dynamics for γ=3 (lower colorscale curve) and 4.95×10^6 s^{-1} (upper color scale curve), n_{bc}=12600, n_{bo}=0.05. D_e=80 cm^2/s, D_h=26 cm^2/s, and w=64 in the simulations in (c,d).(e) Simulated dynamics for D_e=30, 80, and 200 cm^2/s and experimental dynamics for V_g=1.22 V with the rest of the parameters the same as in (d). The electron diffusion constant D_e=80 cm^2/s provides the best fit to the measured dynamics.

generated by the photons with the energy above the bandgap of the $Al_{0.33}Ga_{0.67}As$ layers, can travel in the direction perpendicular to the CQW plane, with some of the carriers being trapped in the CQW. Because the holes are heavier than electrons, the hole trapping to the CQW is more efficient, and therefore an imbalance between holes and electrons in the CQW is created under such photoexcitation. The photoexcited electrons recombine with an equal number of photoexcited holes, producing emission in the vicinity of the excitation spot. At low temperatures and densities, those electrons and holes can bind to form excitons, which can travel away from the excitation spot and cool down to the lattice temperature resulting in the formation of the inner ring in the emission pattern.[7,22,23] The remaining holes, which were photocreated in CQW in excess of the photocreated electrons, diffuse farther away from the laser excitation spot in the CQW plane, as illustrated in Fig. 1(j). The diffusing holes recombine with the ambient electrons present in the entire CQW plane due to an electric current through the structure. This process depletes electrons in the vicinity of the laser spot, creating a hole-rich region. At the same time, a spatial nonuniformity in the electron distribution accumulates, causing a counterflow of electrons toward the laser spot. Excitons created at the interface between the inner hole-rich region and the outer electron-rich region give rise to a ringlike emission pattern, the external ring.

This mechanism of ring formation can be modeled by a system of coupled equations

$$\partial_t n = D_n \nabla^2 n - wnp + \gamma(n_b - n),$$

$$\partial_t p = D_p \nabla^2 p - wnp + I_p \delta(r), \quad (1)$$

with n and p the electron and hole densities, D_e and D_h the diffusion coefficients, and w the rate of electron and hole binding to form an exciton. Hole production at the excitation spot is described by the term $J_h = I_p \delta(r)$. Electron production occurs over the entire plane; the source $J_e = \gamma(n_b - n)$ is given by the difference of the currents in and out of the CQW, with $\gamma(r)$ the electron escape rate and $n_b(r)$ the background electron density in the CQW in the absence of photoexcitation. A stationary solution of Eq. (1), with spatially independent n_b and γ, exhibits electron-rich and hole-rich regions separated by a sharp interface where the exciton density $n_X \propto np$ is peaked, corresponding to the external ring.[8]

Several approximations are used in this model: (i) the hole escape out of the CQW is neglected. This is accurate when the number of escaping holes is small compared to the number of holes recombining with electrons in the CQW. Including such term in Refs. 9–11 results in a qualitatively similar pattern, having little effect on the predicted dynamics of the pattern; (ii) the hole source width is approximated as zero. This is accurate when it is much smaller than the ring diameter; (iii) the diffusion coefficients are approximated as coordinate and density independent; (iv) the electron source is approximated as coordinate independent. The electron source is strongly enhanced at LBS centers in the CQW (see Sec. IV). This approximation is accurate when the ring area contains many LBS.

In addition, we neglect the drift of electrons and holes arising due to the in-plane electric field. To understand when the effect of the drift can be important, let us analyze transport equations for one species, electrons or holes, in the presence of the drift term

$$\frac{\partial n}{\partial t} = D\nabla^2 n - \vec{\nabla} \cdot (\eta \vec{F} n), \quad (2)$$

$$\vec{F} = -\vec{\nabla}(Un), \tag{3}$$

where n is particle density, η is mobility, and $\vec{F}$ is a force describing Coulomb repulsion between particles. In Eq. (3), a short range interaction $U=4\pi e^2 L/\varepsilon$, where L is the distance to the doped region and ε is the dielectric constant, is used to describe the behavior on lengthscales much greater than L, where the value of U is obtained from $U=\frac{2\pi e^2}{\varepsilon k}(1-e^{-2Lk}) \approx \frac{4\pi e^2}{\varepsilon} L$ with $kL \ll 1$. Plugging Eq. (3) in Eq. (2), we find $\partial n/\partial t = D\nabla^2 n + U\eta\vec{\nabla}(n\vec{\nabla}n)$. Comparing the two terms on the right hand side, we see that the drift term is unimportant at densities smaller than

$$n_0 \approx \frac{D}{U\eta} \approx \frac{k_B T\varepsilon}{4\pi e^2 L}, \tag{4}$$

where we have used the Einstein relation $\eta = D/k_B T$.

Using experimental parameter values $T=1.4$ K and $L=200$ nm we obtain $n_0 \approx 10^8$ cm^{-2}. Since the density of electrons and holes is not measured in our experiment, we cannot directly assess the importance of the contribution of the drift term to the carrier transport. However, the agreement between our modeling and the experimental data (see Sec. IV) indicates that the approximation neglecting the carrier drift effect works reasonably well for the studied system.

IV. NUMERICAL SIMULATIONS AND COMPARISON TO EXPERIMENTAL DATA

Here, we employ the model (1) to study the ring dynamics. The solutions of Eq. (1) were used to obtain exciton concentration as $n_X \propto np$. The time-dependent profile of n_X, presented in Fig. 2 along with the experimental data, reproduces all essential features of the observed dynamics: ring expansion, first rapid, then more slow, followed by collapse when the laser source is turned off. The data obtained for different conditions, such as P_{ex} and V_g in Figs. 2(a) and 2(b), were fitted using one set of parameters D_h, D_e, w, and n_b.

The expansion and collapse of the ring occurs on relatively long time scales, in the range of microseconds, controlled by the carrier diffusion in the sample. This is much longer than the tens of nanoseconds estimated for the inner ring, where decay is limited by the exciton lifetime.[23] This sensitivity to diffusion makes the external ring an effective probe of carrier transport.

An increase in the amount of holes created by a higher laser excitation results in an increase in both the ring radius and the collapse time [Fig. 2(a)]. In contrast, increasing gate voltage results in an increase in the number of ambient electrons, which reduces both the ring radius and the collapse time [Fig. 2(b)]. These dependences, observed in experiment, are borne out by the simulations.

The parameters in simulations were chosen to fit the ring radius R at the laser pulse end and the ring collapse time τ_R, evaluated as the time it takes for the radius to drop by 50%. The simulations show that R and τ_R depend strongly on some of the parameters, e.g., the hole and electron sources in Eq. (1), and weakly on the others, e.g., the exciton formation rate w or electron diffusion coefficient D_e, see the Appendix.

Our task was made simpler because the radius R is essentially independent of the hole diffusion coefficient [Fig. 2(d)]. This can be understood from the continuity equation for hole transport in a steady state: for large R, the hole flux at the ring becomes independent of D_h since an increase in D_h leads to a corresponding reduction in the density gradient conserving the total hole flux.[25] In contrast, the collapse time τ_R depends strongly on D_h and relatively weakly on D_e [Fig. 2(e)], since the electron source is spread everywhere in the CQW plane, while holes are only created in the laser spot and have to travel to the ring from there. These observations can be used to estimate D_h from the observed ring dynamics: First, the sources can be determined by fitting the ring radius, then D_h becomes the main parameter determining τ_R, so that it can be estimated from fitting the measured τ_R. The best fit gives an estimate $D_h \approx 26$ cm^2/s (Figs. 2(c) and 2(e)).

Now we analyze the dynamics of LBS rings (Fig. 3), which are centered around electron current filaments.[8] Each such filament represents a local electron source creating an electron-rich region, surrounded by a hole-rich region inside the external ring. The interface between the hole-rich and electron-rich regions is seen as an LBS ring in exciton emission [see schematic in Fig. 1(j)]. The LBS-ring dynamics after the laser pulse was modeled by Eq. (1) with electron source peaked at the LBS center: $n_b(r \le r_0) = n_{bc}$, $n_b(r > r_0) = n_{bo}$. We used $r_0 = 0.26$ μm, which is smaller than the experimental resolution. The results were not sensitive to the choice of r_0.

When the laser is turned off, the hole source is terminated and the electrons injected by the current filament travel outwards expanding an electron-rich region around the LBS center and pushing the electron-hole interface away from it. This results in the expansion of the LBS ring (Fig. 3). Figures 3(a)–3(c) show that a brighter LBS expands faster. Since the LBS 1, 2 and 3 are at essentially the same distance from the laser spot and thus have a similar hole density around them, this behavior originates from a larger electron source for a brighter LBS. We observe faster LBS-ring expansion for higher gate voltage V_g [Fig. 3(d)]; this originates from a larger electron source for a higher V_g. These dependences are consistent with those found in simulations. Since for LBS formation the roles of electrons and holes interchange, the LBS expansion and collapse dynamics can be used to determine the electron diffusion coefficient D_e in a manner similar to the external ring dynamics used to determine D_h. The local electron source at the LBS center, which dominates the initial expansion of the LBS ring, can be determined from measured initial expansion speed. Following the steps outlined above we arrive at an estimate $D_e \approx 80$ cm^2/s.

V. SUMMARY

In summary, we studied exciton front propagation in photoexcited GaAs quantum wells seen as expanding and collapsing exciton rings in exciton emission patterns. The measurements of the front propagation velocity are used to estimate the electron and hole diffusion coefficients.

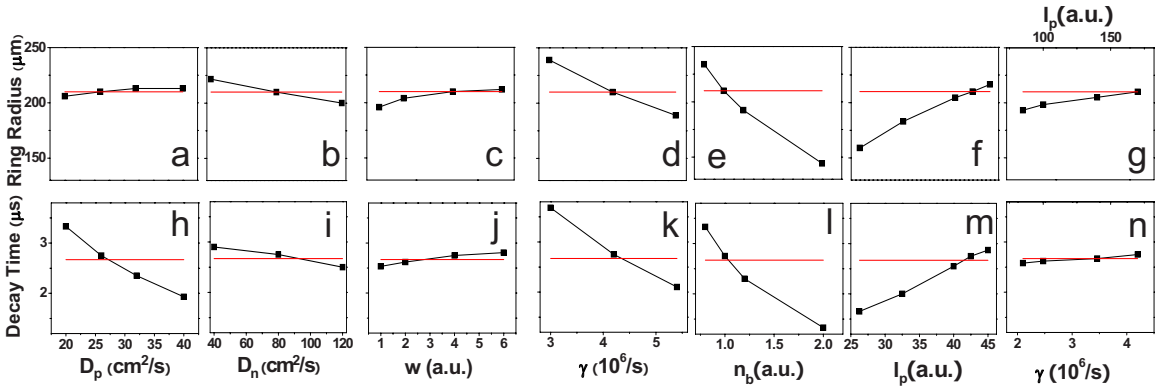

FIG. 4. (Color online) (a–g) Radius and (h–n) collapse time of the external ring as a function of parameters in the simulations. (a–f, h–m) One parameter is varied while the others are kept at the values presented for the top curve in Fig. 2(a). D_p and D_n are the hole and electron diffusion coefficients, w electron-hole binding rate, γ electron escape rate, n_b background electron density in the CQW in the absence of photoexcitation, and I_p hole production rate in the excitation spot. (g,m) I_p and γ are varied simultaneously keeping the ratio I_p/γ constant while the other parameters are kept at the values presented for the top curve in Fig. 2(a).

ACKNOWLEDGMENTS

This work is supported by ARO and NSF.

APPENDIX

Unit calibration. The model includes the units of length, time, and particle number. The units in simulations L, T, and N correspond to the real units in experiments L', T', and N' with the rescaling factors $C_L=\frac{L'}{L}$, $C_T=\frac{T'}{T}$, $C_N=\frac{N'}{N}$.

Experimental data for $P_{ex}=1.82$ mW, which produces the ring with the radius $R'=200$ μm in the experiment, correspond to the simulation with $I_p=42.5$ and $R=8$, see Fig. 2(a). This yields $C_L=\frac{R'}{R}=25$ μm. The laser pulse width in the experiments $T'=10$ μs corresponds to $T=300$ in the simulations. Therefore $C_T=\frac{T'}{T}=3.3\times10^{-2}$ μs. The determination of C_N requires the measurement of either the formation rate of excitons or the current through the structure, see below. It is not done in the present work.

In the Eq. (1) used in the simulations, all parameters are in the simulation units. The equation should keep its form when the units are changed to real. The rescaling relationships for the terms in the equation are: $\partial_t=C_T\partial_{t'}$, $\nabla^2=C_L^2\nabla'^2$, $n=\frac{C_L^2}{C_N}n'$, $I=\frac{C_T}{C_N}I'$, $\delta(\vec{r})=C_L^2\delta(\vec{r}')$. Plugging them to Eq. (1) yields

$$\frac{C_TC_L^2}{C_N}\partial_{t'}n'=\frac{C_L^4}{C_N}D_n\nabla'^2n'-\frac{C_L^4}{C_N^2}wn'p'+\frac{C_L^2}{C_N}\gamma(n_b'-n'),$$

$$\frac{C_TC_L^2}{C_N}\partial_{t'}p'=\frac{C_L^4}{C_N}D_p\nabla'^2p'-\frac{C_L^4}{C_N^2}wn'p'+\frac{C_TC_L^2}{C_N}I_p'\delta(\vec{r}'). \tag{A1}$$

Comparing Eq. (A1) with the equation in real units

$$\partial_{t'}n'=D_n'\nabla'^2n'-w'n'p'+\gamma'(n_b'-n'),$$

$$\partial_{t'}p'=D_p'\nabla'^2p'-w'n'p'+I_p'\delta(\vec{r}'), \tag{A2}$$

gives the rescaling relationships for the coefficients

$$D_n'=\frac{C_L^2}{C_T}D_n=200\ \text{cm}^2/\text{s}\times D_n,$$

$$D_p'=\frac{C_L^2}{C_T}D_p=200\ \text{cm}^2/\text{s}\times D_p,$$

$$w'=\frac{C_L^2}{C_TC_N}w=\frac{200\ \text{cm}^2/\text{s}}{C_N}\times w,$$

$$\gamma'=\frac{1}{C_T}\gamma=3\times10^7/\text{s}\times\gamma. \tag{A3}$$

As described in Sec. IV, D_n can be obtained from the LBS-ring kinetics and D_p—from the external ring kinetics. The other parameters are briefly discussed below. The parameter describing the electron source γ can be obtained from both LBS and external ring measurements as described in Sec. IV. Our simulations show that varying the exciton formation rate w affects the ring width but practically does not change the ring radius and decay time. Therefore, w was not determined from the data. The determination of the density $n=\frac{C_L^2}{C_N}n'$ requires the evaluation of C_N. In turn, C_N can be determined by measuring the electron current through the sample in the absence of photoexcitation. However, the current in the experiments is small and its measurement is beyond the scope of this work (total leakage current in the structure is <1 μA for the excitations above the AlGaAs gap and below the instrumentation sensitivity 10 nA for resonant or no excitation).

Fitting procedure. There are six parameters in Eq. (1): diffusion coefficients D_n and D_p; exciton formation rate w; and source terms presented by I_p, γ, and n_b. For C_N unknown, we set $n_b=1$. We probed the dependence of the ring radius and collapse time on each other parameter, see Fig. 4.

Varying the exciton formation rate w practically does not change the ring radius R and collapse time τ_R, see Figs. 4(c) and 4(j). Varying I_p and γ simultaneously keeping $I_p/(\gamma n_b)$

constant only weakly changes R (consistent with the conclusions of Ref. 11) and τ_R, see Figs. 4(g) and 4(n).

In our fitting procedure for the external ring, we first determined the sources by fitting R, see Figs. 4(d)–4(f). Then D_h becomes the parameter, which determines the ring collapse time, so that it can be estimated from fitting the measured τ_R. The best τ_R gives an estimate $D_h \approx 26$ cm^2/s, see Fig. 4(h). Both R and τ_R are only weakly sensitive to D_n, see Figs. 4(b) and 4(i). The estimate for $D_n = 80$ cm^2/s was obtained by fitting the kinetics of LBS rings, see Sec. IV. In turn, the obtained values of D_n and D_p were used in estimating γ, n_b and I_p by fitting the ring radius, Figs. 4(d)–4(f), embracing the procedure.

The procedure for LBS was similar. The ratio of sources was obtained by fitting the initial LBS-ring expansion between $t=0$ and 1 μs. Then D_n was estimated by fitting the expansion at $t>1$ μs.

The false color plots presenting the simulations in the paper show the value $n \times p$, which is proportional to the exciton density. To combine several simulation results in one figure, we present the maximum value in the simulations for each time.

[1] H. J. Prager, K. K. N. Chang, and S. Weisbrod, Proc. IEEE **55**, 586 (1967).
[2] I. V. Grekhov, Solid-State Electron. **32**, 923 (1989).
[3] R. J. Focia, E. Schamiloglu, C. B. Fleddermann, F. J. Agee, and J. Gaudet, IEEE Trans. Plasma Sci. **25**, 138 (1997).
[4] P. Rodin, U. Ebert, A. Minarsky, and I. Grekhov, J. Appl. Phys. **102**, 034508 (2007).
[5] J. B. Benziger, E.-S. Chia, Y. De Decker, and I. G. Kevrekidis, J. Phys. Chem. C **111**, 2330 (2007).
[6] S. Jakubith, H. H. Rotermund, W. Engel, A. von Oertzen, and G. Ertl, Phys. Rev. Lett. **65**, 3013 (1990).
[7] L. V. Butov, A. C. Gossard, and D. S. Chemla, Nature (London) **418**, 751 (2002).
[8] L. V. Butov, L. S. Levitov, A. V. Mintsev, B. D. Simons, A. C. Gossard, and D. S. Chemla, Phys. Rev. Lett. **92**, 117404 (2004).
[9] R. Rapaport, G. Chen, D. Snoke, S. H. Simon, L. Pfeiffer, K. West, Y. Liu, and S. Denev, Phys. Rev. Lett. **92**, 117405 (2004).
[10] G. Chen, R. Rapaport, S. H. Simon, L. Pfeiffer, and K. West, Phys. Rev. B **71**, 041301(R) (2005).
[11] M. Haque, Phys. Rev. E **73**, 066207 (2006).
[12] L. M. Smith, J. S. Preston, J. P. Wolfe, D. R. Wake, J. Klem, T. Henderson, and H. Morkoc, Phys. Rev. B **39**, 1862 (1989).
[13] U. Sivan, P. M. Solomon, and H. Shtrikman, Phys. Rev. Lett. **68**, 1196 (1992).
[14] J. P. Eisenstein, G. S. Boebinger, L. N. Pfeiffer, K. W. West, and S. He, Phys. Rev. Lett. **68**, 1383 (1992).
[15] T. S. Lay, Y. W. Suen, H. C. Manoharan, X. Ying, M. B. Santos, and M. Shayegan, Phys. Rev. B **50**, 17725 (1994).
[16] A. H. MacDonald, Physica B **298**, 129 (2001).
[17] V. Pellegrini, S. Luin, B. Karmakar, A. Pinczuk, B. S. Dennis, L. N. Pfeiffer, and K. W. West, J. Appl. Phys. **101**, 081718 (2007).
[18] L. Tiemann, J. G. S. Lok, W. Dietsche, K. von Klitzing, K. Muraki, D. Schuh, and W. Wegscheider, Phys. Rev. B **77**, 033306 (2008).
[19] A. F. Croxall, K. Das Gupta, C. A. Nicoll, M. Thangaraj, H. E. Beere, I. Farrer, D. A. Ritchie, and M. Pepper, Phys. Rev. Lett. **101**, 246801 (2008).
[20] J. A. Seamons, C. P. Morath, J. L. Reno, and M. P. Lilly, Phys. Rev. Lett. **102**, 026804 (2009).
[21] In this paper, transport of electrons or holes in one layer is probed essentially in the absence of carriers in the other layer.
[22] A. L. Ivanov, L. E. Smallwood, A. T. Hammack, Sen Yang, L. V. Butov, and A. C. Gossard, EPL **73**, 920 (2006).
[23] A. T. Hammack, L. V. Butov, J. Wilkes, L. Mouchliadis, E. A. Muljarov, A. L. Ivanov, and A. C. Gossard, Phys. Rev. B **80**, 155331 (2009).
[24] See supplementary material at http://link.aps.org/supplemental/10.1103/PhysRevB.81.115320 for a movie showing the front propagation of the expanding and collapsing rings in the emission pattern of indirect excitons.
[25] Formula (3) in Ref. 8 for the ring radius contains a typo, which has been corrected in Eq. (8) in Ref. 11.